ISSN 0001-4370, Oceanology, 2013, Vol. 53, No. 2, pp. 211–222. © Pleiades Publishing, Inc., 2013.
Original Russian Text © E.A. Ovsepyan, E.V. Ivanova, L. Max, J.-R. Riethdorf, D. Nürnberg, R. Tiedemann, 2013, published in Okeanologiya, 2013, Vol. 53, No. 2, pp. 237–248.

MARINE GEOLOGY

# Late Quaternary Oceanographic Conditions in the Western Bering Sea

**E. A. Ovsepyan[a], E. V. Ivanova[a], L. Max[b], J.-R. Riethdorf[c], D. Nürnberg[c], and R. Tiedemann[b]**

[a]*Shirshov Institute of Oceanology, Russian Academy of Sciences, pr. Nakhimovskii 36, Moscow, 117997 Russia*
*e-mail: ameli_cat@mail.ru, e_v_ivanova@ocean.ru*
[b]*Alfred Wegener Institute for Polar and Marine Research, Bremerhaven, Germany*
[c]*GEOMAR Helmholtz Centre for Ocean Research (Kiel), Kiel, Germany*

Received July 14, 2011; in final form, August 10, 2012

**Abstract**—The benthic and planktonic foraminiferal assemblages and the distribution of coarse grain-size factions were studied in the upper 4.5 m of the Core SO201-2-85KL (57°30.30′ N, 170°24.79′ E, water depth 968 m) retrieved from the Shirshov Ridge. This part of the core covers 7.5 to 50 kyr BP. The glacial period is established to be characterized by low surface water productivity, the wide distribution of sea ice and/or icebergs in this area, and a high oxygen concentration in the bottom layer. Enhanced productivity is inferred from the maximum abundance of planktonic foraminifers at the very beginning of the deglaciation. The late Bølling–Allerød interstadial and the early Holocene were marked by the further two-phase increase in the surface productivity and the weakened ventilation of the bottom water.

**DOI:** 10.1134/S0001437013020136

## INTRODUCTION

The significant role of the Bering Sea in the heat and water exchange between the Pacific and Arctic Oceans and its proximity to the poorly known Northern Pacific terminus of the global oceanic conveyor stimulated enhanced efforts of international scientific teams in investigating this region during the 21st century. The Bering Sea is one of the most productive basins in the World Ocean with maximal primary production values ranging from 250–500 gC/cm$^2$ per year above the continental slope to 50–100 gC/cm$^2$ per year above the Shirshov Ridge [37] despite of the deficiency of Fe in the euphotic layer [27].

It was established that the biological productivity of the surface water layer in the Bering Sea was low during the glacial marine isotopic stages (MIS) 3–2 [7, 8, 17, 18, 25, 26]. According to the geochemical and micropaleontological (benthic foraminiferal) data, the Bølling–Allerød interstadial and the early Holocene were marked by a two-step increase of the sea surface productivity in the southern and northern parts of the basin [17, 18, 26]. A similar inference was derived from the geochemical data and diatom analysis for its western part as well [12, 16]. It was also shown that the same periods were characterized by weakened ventilation of the bottom water in the northern and western parts of the sea at intermediate depths [12, 26]. In the southern part of the basin at a depth of 3060 m, calcareous microfossils appeared to be completely dissolved in the sediments deposited during the last ~3 kyr [7, 8]. The lysocline and CCD over the continental slope of the Bering Sea are documented at depths of 2000 and 3800 m, respectively [11]. Information on the ecology, biogeography, and quantitative distribution of the benthic foraminifers (BF) is available from [3, 6]. The data on the distribution of the planktonic foraminifers (PF) in the recent sediments of the northwestern (subarctic) Pacific Ocean and Bering Sea are scarce.

The Core SO201-2-85KL (57°30.30′ N, 170°24.79′ E, water depth 968 m, Fig. 1) was retrieved from the Shirshov Ridge during the cruise 201-2 of the R/V *Sonne* carried out in the framework of the Russian–German KALMAR Project in 2009. The age model of the upper part of the core is based on visual correlation between the color reflectance b* curve and the oxygen isotope curve of the Greenland NGRIP ice core and supported by seven AMS $^{14}$C dates [31, 34], five of which were obtained for the Core SO201-2-85KL. Two dates (10.3 and 11.2 kyr BP) correspond to the average age values for two Ca intensity peaks in the X-ray fluorescence spectra obtained for this and several other cores from the northwestern Pacific. All the radiocarbon dates are recalculated into calendar years using the reservoir age of 700 years (Fig. 2), which is accepted to be constant for the last 25 kyr [31]. The following stratigraphic units, which are generally used in the paleoceanographic and paleogeographic correlations, are defined in accordance with this chronostratigraphic framework (Fig. 2): the interstadial of the last glaciation (50.0–28.6 kyr BP; 446–226 cm); the stadial (including the Last Glacial Maximum (LGM)), 28.6–20.0 kyr BP, 226–136 cm); the early deglaciation (20.0–14.8 kyr BP, 136–80 cm); the

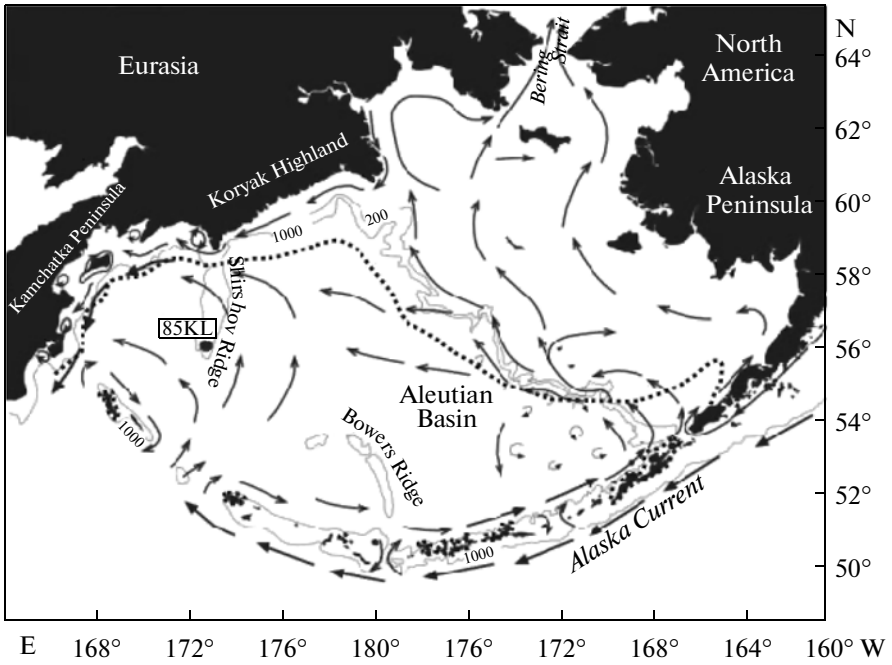


**Fig. 1.** Surface circulation in the Bering Sea (after [38]) and core location on the Shirshov Ridge. The dotted line shows the maximum of sea ice extent in January–March of 2008 [42].

Bølling–Allerød (14.8–12.9 kyr BP, 80–59 cm); the Younger Dryas (12.9–11.7 kyr BP, 59–52 cm); and the early Holocene (11.7–9.2 kyr BP, 52–16 cm).

This work is aimed at reconstructing the sea surface bioproductivity and bottom-water ventilation at intermediate depths in the western Bering Sea from the interstadial of the last glaciation (MIS 3) to the mid-Holocene (MIS 1) based on the study of the millennium-scale variability of the benthic and planktonic foraminiferal assemblages. The variations in content and composition of coarse fractions allow us to reconstruct sea ice conditions in the Core SO201-2-85KL area.

## OCEANOGRAPHIC SETTING

In the Bering Sea, the surface circulation is mainly determined by the cyclonic cell, which represents an element of the large Subarctic gyre (Fig. 1). The surface Alaska Current penetrates into the basin via the straits in the Aleutian island arc and, being transformed, flows northward along the continental slope. A minor part (0.8 Sv) of the transformed water outflows to the Arctic Ocean through the Bering Strait [38].

In the deep part of the Bering Sea, the water column consists of the following layers: (1) the surface mixed layer heated in the summer (0 to 25–50 m, 7–10°C, 33‰) [1]; (2) the subsurface cold Bering Sea water (150–200 m, 1.5–2.0°C, 31.5–33.0‰); (3) the North Pacific Intermediate Water (200–500 m, 3.4–4.0°C, 33.7–34.1‰) [30] in the upper part of the mesothermal layer (200–2000 m) [14]; and (4) the deep water (>2000, 1.45–1.65°C, 34.60–34.68‰) which is represented by a mixture of deep and bottom waters of Antarctic and North Atlantic origin [14]. The oxygen minimum zone is located at depths of 300–900 m, being characterized by dissolved oxygen concentrations of ~0.34 mL/L in its lower part [35].

According to the satellite altimetry data [42], the seasonal ice cover is developed mostly in the northern and eastern parts of the basin and is absent over the Shirshov Ridge (Fig. 1).

## MATERIALS AND METHODS

In this work, we use the on-board visual lithological description of the Core SO201-2-85KL [14], our grain-size distribution data obtained using SediGraph 5100 equipment and the coarse fraction (>63 μm) content measured by the mesh analysis.

The samples for the foraminiferal analysis were taken on board every 5 cm. After the cruise, they were

**Fig. 2.** Multiproxy time series for the Core SO201-2-85KL. The stratigraphy and chronology are after [31, 34]. (BF) benthic foraminifers; (PF) planktonic foraminifers; (MIS) marine isotopic stages; (YD) Younger Dryas; (B/A) Bølling/Allerød interstadial; (LGM) Last Glacial Maximum. The gaps in plots of the *N. pachyderma* sin. and *G. bulloides* relative abundances indicate insufficient PF contents.

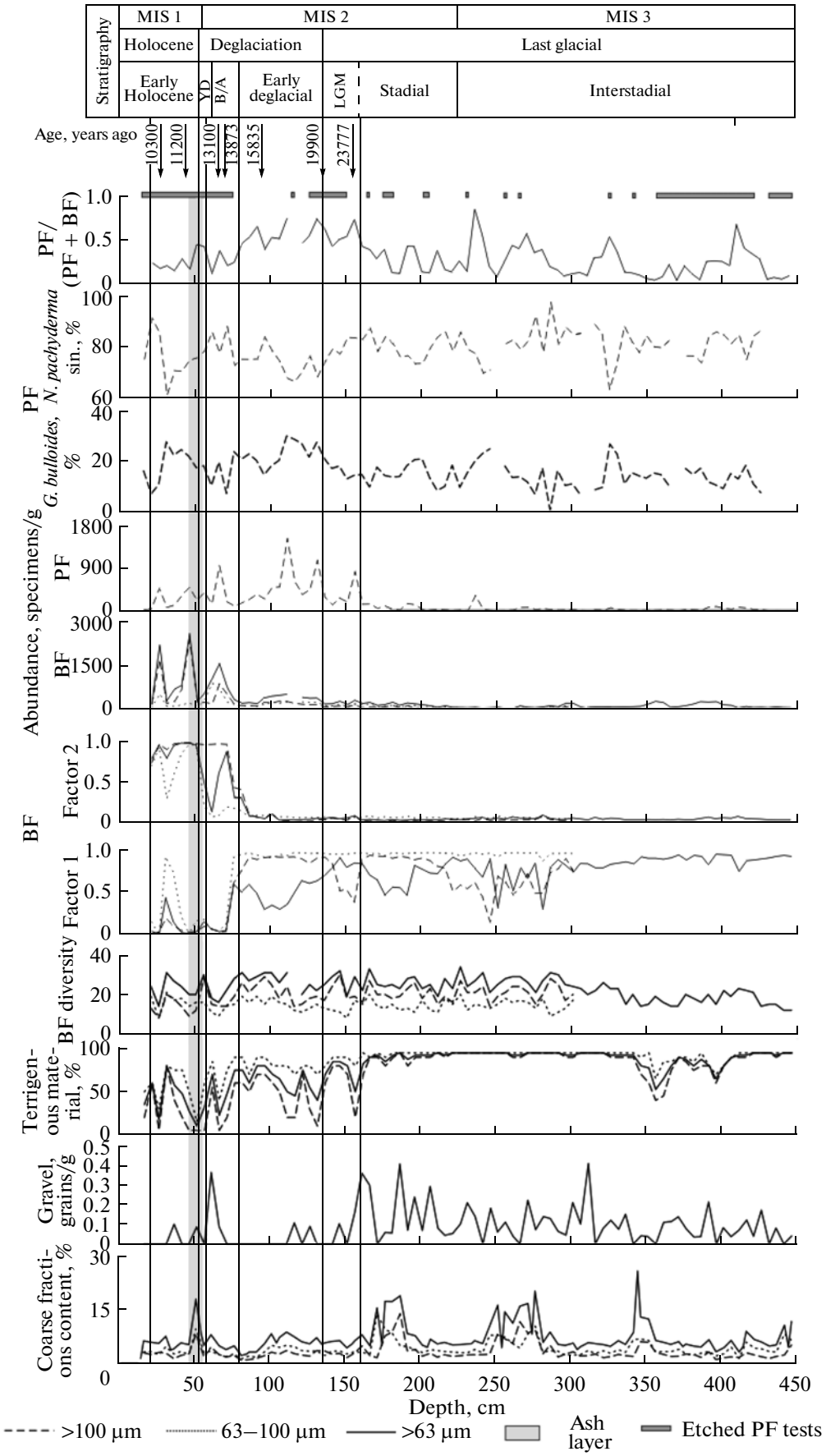
Stratigraphy
MIS 1
MIS 2
MIS 3
Holocene
Deglaciation
Last glacial
Early Holocene
YD
B/A
Early deglacial
LGM
Stadial
Interstadial
Age, years ago
10300
11200
13100
13873
15835
19900
23777
PF/ (PF + BF)
PF
N. pachyderma sin., %
G. bulloides, %
Abundance, specimens/g
PF
BF
BF
Factor 2
Factor 1
BF diversity
Terrigenous material, %
Gravel, grains/g
Coarse fractions content, %
Depth, cm
>100 μm
63–100 μm
>63 μm
Ash layer
Etched PF tests

stored for three months under a temperature of 4°C in a refrigerator at Sirshov Institute of Oceanology of the Russian Academy of Sciences. Then, they were washed with distilled water over 63 and 100 μm-mesh sized sieves and dried at room temperature. The dried coarse fractions were weighted for calculation of their proportion. The contents of the terrigenous grains, biogenic fragments and volcanogenic clasts were visually estimated with accuracy up to 5% in both fractions of each sample and subsequently recalculated for the >63 μm size fraction. The >100 μm size fraction was sieved over a 1000 μm-mesh size sieve to separate the gravel grains and then to calculate their concentration in a sample. Dry fractions were splitted by an Otto microsplitter to obtain 100–300 PF specimens and 250–300 BF tests. The PF tests were counted only in the >100 μm fraction because most samples of 63–100 μm size fraction contained only their fragments. In the upper 3 m of the core, quantitative analyses of BF assemblages were carried out in both the 63–100 and >100 μm size fractions to reveal differences between the test size distribution. Below this level, the BF were analyzed in the >63 μm size fraction. In addition, the number of PF and BF tests per unit gram were calculated on the basis of counted number and dry weight. Biodiversity, i.e., the number of BF species, was counted in each sample. The dissolution of PF and BF tests was estimated visually and using the PF/(BF+PF) ratio. To obtain the dominant BF assemblages, the CABFAC factor analysis was applied for the species percentages matrix [21] containing no less than 2% of each species. In order to reconstruct variations of the oxygen content in bottom and pore waters, the BF species were subdivided into oxic, suboxic B, suboxic C, and dysoxic groups depending on their tolerance to oxygen concentrations in the bottom water using the technique [24] and the classification [2] for the Sea of Okhotsk. The Fe/S ratios are calculated using the data of the X-ray fluorescence analysis. This proxy serves as an independent indicator of the redox conditions in the surface sediment layer during the early diagenesis stage, which indirectly reflects intensity of the bottom water ventilation [39]. The X-ray fluorescence analysis (XRF) of the core was conducted at the Alfred Wegener Institute for Polar and Marine Research (Germany) using a sample resolution of 1 cm and 30 s count time.

## RESULTS

**Lithology and stratigraphy.** The following layers are defined in the core section (from the base upward): (1) diatomaceous ooze, light greenish gray, soft, intensely disturbed (especially in the upper 16 cm) by coring (0–30 cm); (2) sandy-clayey silt, terrigenous, enriched in foraminifers and mixed with diatomaceous ooze owing to coring disturbance (30–47 cm); (3) black layer of volcanic ash (47–55 cm); (4) visually uniform dark olive-gray terrigenous sediments represented by intercalating of vague beds of — sandy-silty clay (55–226, 290–320, 360–430 cm) and sandy-clayey silt (226–290, 320–360, 430–450 cm). The upper 70 cm of the core contains diatoms. Below 130 cm, the sediments exhibit dark spots of hydrotroilite, the abundance of which increases downward. Inasmuch as the upper 16 cm of the sediments are intensely disturbed by the coring, the corresponding data are omitted from the further analysis.

The content of coarse (>63 μm) fraction represented by the terrigenous; biogenic (foraminiferal tests, diatom frustules, radiolarian skeletons); and, locally, volcanoclastic material in the studied part of the core varies from 3 to 7% with an increase up to 20–25% in some intervals (Fig. 2). The high amount (50–95%) of terrigenous material in the >63 μm size fraction is estimated in the sediments corresponding to MIS 3, the early MIS 2, and the LGM (Fig. 2). In the sediment of the early and late parts of Bølling/Allerød and the early deglacial, its proportion ranges from 40 to 80%. In the mid-Bølling/Allerød interstadial, the amount of terrigenous particles in this fraction constitutes 22%; in the early Holocene, it varies from 10 to 80%. The content of gravel fraction represented by subangular and angular rock fragments of 1–10 mm slightly varies between 0 and 0.4 grain/g (Fig. 2).

High Fe/S values, a proxy of buried oxidized sediments [39], are typical for MIS 3, the MIS 2 stadial, the Younger Dryas, and the mid-Holocene sediments (Fig. 3).

**Planktonic foraminifers.** The PF abundance is generally low and in some cases insufficient for reliable quantitative analysis (<100 specimens/sample). However, it reaches high values (>700 specimens/g of dry sediment) within MIS 2 with two maxima at the very onset of deglaciation (>1500 specimens/g, Fig. 2). This interval is characterized by the best preservation of the PF tests, low concentrations of their fragments, and the high PF/BF ratio. The strongest dissolution of PF tests is recorded in the sediments of Bølling/Allerød interstadial, Holocene, and some intervals of MIS 3 (Fig. 2).

The PF assemblages consist of six species typical of this region [8, 28]. A dominance of the polar species *Neogloboquadrina pachyderma* sin. (61–91% of the total abundance in the assemblage) is recorded throughout the studied part of the core. In the North Atlantic and Arctic oceans the species generally dwells in the upper 20–100 m of the water column depending on the depth of the subsurface chlorophyll maximum [28]. The variations in percentages of *N. pachyderma* sin. and boreal species *Globigerina bulloides* (second in abundance, 0–30%), an indicator of enhanced bioproductivity [17, 33], demonstrate antiphase oscillations without any relation to stratigraphic units defined in the core (Fig. 2). Other boreal species (*Turborotalita quinqueloba, Neogloboquadrina pachyderma* dex., *Globigerinita uvula*, and the cosmopolitan *Globigerinita glutinata*) constitute 0–11% (usually < 5%) of

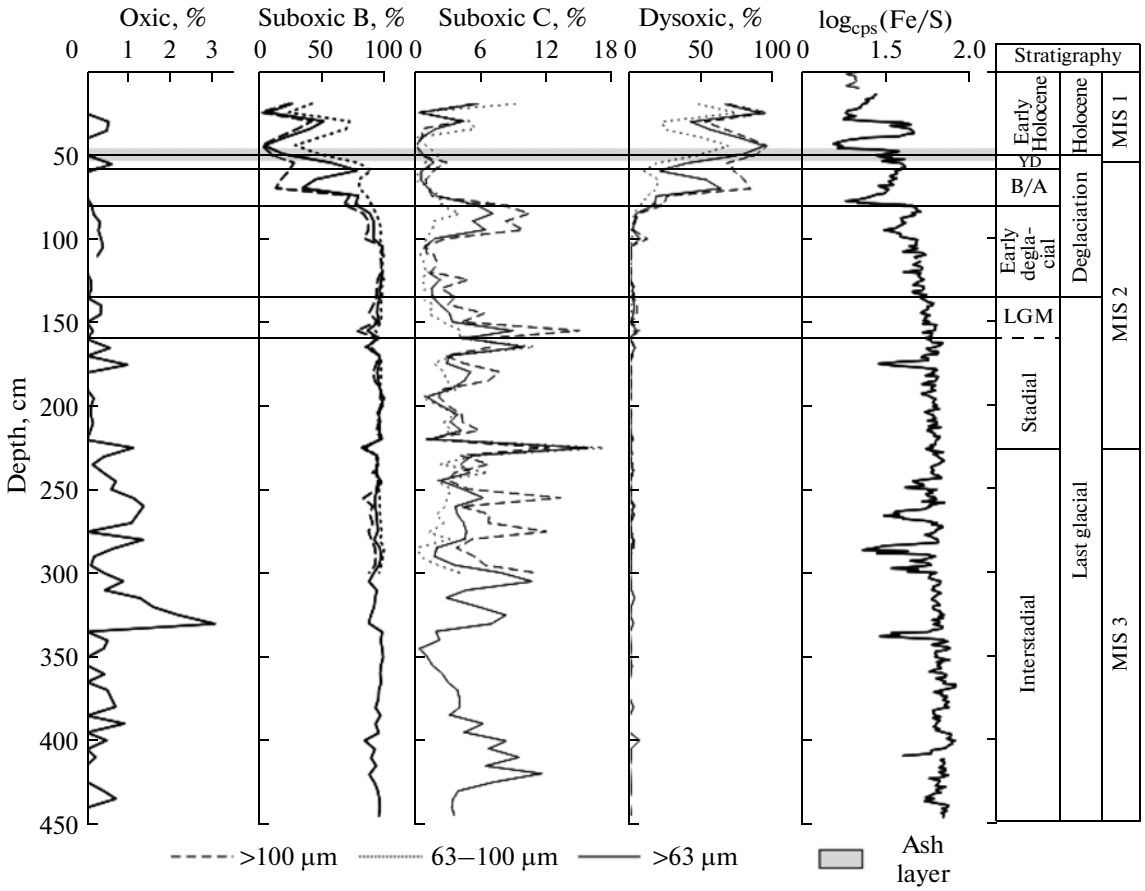


**Fig. 3.** The distribution of oxygen-related groups of benthic foraminifers after [2, 24] in >100, 63–100, and >63 μm size fractions and the variations of the Fe/S values indicating the redox conditions. $\log_{cps}$ (Fe/S)—the XRF element intensities. For the legend, see Fig. 2.

the assemblage. Scarce specimens of the tropical species *Globigerinoides ruber* were found in sediments of MIS 3 (at 240 and 248 cm).

**Benthic foraminifers.** The BF assemblage from the studied interval of the core SO201-2-85KL includes 79 species. In our reconstructions, we focused on the distribution of the ecologically indicative species for which the ecology and microhabitat were previously described (Fig. 4). The BF assemblage from the >63 μm size fraction of the glacial sediments consists of *Alabaminella weddellensis* (an opportunistic species indicating the seasonal influx of fresh organic matter to the bottom) [e.g., 41], *Islandiella norcrossi* (up to 50%), the Arctic form preferring cold bottom water with relatively high and stable salinity [29], *Angulogerina angulosa* (0–20%), an indicator of high-energy bottom-water hydrodynamics [3], and large thick-walled *Islandiella californica* (up to 12%), a proxy of well oxygenated bottom water [24]. The relative abundance of *Cassidulina norvangi*, which is in our opinion a synonym of the cold-resistant form *Cassidulina reniforme* [19], constitutes 0–12% of the glacial assemblage. The typical postglacial species *Bulimina tenuata* (10–55%) and *Bolivina seminuda* (5–50%) are indicators of high bioproductivity tolerant to an oxygen deficiency [41]. *B. seminuda* is able to survive under strong oxygen-depleted conditions (up to <0.1 mL/L) [36]. In the sediments of the early deglaciation the proportion of *Elphidium batialis* increases up to 12% (Fig. 4). This species is abundant in the recent sediments of the Shirshov Ridge [6] with $C_{org}$ concentrations exceeding 2% [5]. The presence of well oxygenated bottom water is an important factor favoring the proliferation of *Elphidium batialis* [3]. The relative abundance of *Uvigerina akitaensis* (0–30%) occurring throughout the studied interval in 63–100 and >100 μm size fractions varies without any visible correlation with the stratigraphic units .

The factor analysis reveals that the variability of taxonomic composition is described by two factors, which together explain 86.7, 90.4, and 85.6% of the variance in >63, 63–100, and >100 μm size fractions, respectively. Factor 1 is dominated by the following main species: *A. weddellensis* (factor loadings are 0.87 and 0.96) and *I. norcrossi* (0.45 and 0.24) in >63 and 63–100 μm size fractions, respectively, and *I. norcrossi* (0.87) in the >100 μm size fraction. The dominant species of Factor 2 are *B. tenuata* (0.66 and 0.57)

and *B. seminuda* (0.65 and 0.49) in >63 and >100 μm size fractions, respectively, and *Pseudoparella suttuensis* (0.65), *Fursenkoina* spp. (0.50), and *B. tenuata* (0.42) in the 63–100 μm size fraction (Figs. 2, 4). Since the middle part of Bølling/Allerød interstadial, the "glacial" BF assemblage (Factor 1) is replaced by the postglacial one (Factor 2). The BF diversity slightly varies throughout the section. The most notable increase in their diversity is documented in the middle part of the MIS 3–2: from 16–20 to 25–29 species.

The interval from MIS 3 to the mid-Bølling/Allerød is characterized by the common occurrence of the suboxic B group of benthic foraminifers (table), which content constitutes not less than 65% in each fraction (Fig. 3). The oxic group proportion never exceeds 3% throughout the studied part of the core. The relative abundance of the dysoxic group (table) in the 63–100, >100, and >63 μm size fractions increases from a few percents during the glacial to 20, 85, and 64%, respectively in mid-Bølling/Allerød and to 70, 97 and 95% respectively, in the early Holocene. The content of the dysoxic group in the same fractions decreases to 11.68 and 21%, and the share of suboxic B group increases to 89.28 and 78% respectively, at the transition from the Bølling/Allerød interstadial to the Younger Dryas stadial.

## PALEOCEANOGRAPHIC RECONSTRUCTIONS

The following proxies were used to reconstruct the paleoceanographic conditions in the Shirshov Ridge area: total PF and BF abundances, the percentages of the indicative species, the oxygen-related BF groups, and the terrigenous material content and concentrations of gravel-sized rock clasts. The synchronous distribution of the independent parameters in the continuous sedimentary sequence allows us to reconstruct the oceanographic environments in the western Bering Sea from the last interstadial to the mid-Holocene (Figs. 2, 3). The Younger Dryas is represented by a single sample and is omitted from the further consideration.

The dominance of polar species *N. pachyderma* sin. in PF assemblages of the Core SO201-2-85KL suggests a prevalence of cold conditions in the subsurface water through the time interval studied (Figs. 2, 5). The absence of an unambiguous correlation between the stratigraphic units and the relative abundance of the two dominant PF species (*N. pachyderma* and *G. bulloides*) might be explained by the recently established adaptation of the North Pacific *N. pachyderma* sin. genotype (VII) to somewhat warmer temperature range as compared to the North Atlantic counterpart (genotype I) [13]. According to numerous observations, *G. bulloides* is considered to be a boreal species, i.e. adopted to warmer-waters as compared to *N. pachyderma* sin., and as well indicative of high primary production [e.g., 17, 33]. The rare specimens of the tropical species *G. ruber* found in the sediments of MIS 3 were likely transported by warm surface currents from the North Pacific through straits in the Aleutian island arc.

**Paleoproductivity.** To reconstruct the surface water paleoproductivity we used the proxies widely applied in recent studies: the total PF and BF abundances [e.g., 18] and the percentages of the indicative BF [7, 41] and PF [8, 17] species.

The comparative quantitative analysis of the BF assemblages in the 63–100 and >100 μm size fractions revealed that seasonal pulses of organic matter flux inferred from the dominance of *A. weddellensis* [41], can be ascertained only in the 63–100 μm size fraction (Fig. 4). Thus, the most complete information on paleoproductivity in this region might be inferred from the sum fraction of >63 μm.

An increase in percentages (up to 25%) of the planktonic *G. bulloides* (Fig. 2) and the benthic *I. norcrossi* (Fig. 4), which prefers moderate organic matter flux, implies relatively low surface-water productivity during MIS 3, MIS 2, and LGM prior to 20 kyr BP. Meanwhile, the low total abundances of both the planktonic and benthic foraminifers (Fig. 2) most likely point to a low bioproductivity. The insufficient food resources might be explained in terms of low phytoplankton production due to a nutrient deficiency in the euphotic layer [22]. The short and relatively cold summer seasons might limit the annual phytoplankton production as well. Nevertheless, the relative abundance of the opportunistic species *A. weddellensis* (Fig. 4) was high even in the case of strong pulsed fluxes of fresh organic matter to the bottom during short seasonal phytoplankton blooms at MIS 3–LGM. We assume that the habitats were intermittently more suitable for the mixed-layer dwelling species *G. bulloides*, than for the relatively deep dwelling *N. pachyderma* sin. The favorable conditions might lead to an increase of *G. bulloides* abundance in many samples from the MIS 3–LGM time span. This finding is in line with the high (up to 40%) values of *G. bulloides* during MIS 3 on the Bowers Ridge located in the southern part of the sea [17]. The PF abundance peak at LGM (Fig. 2) indicates some increase in the primary production caused by the supply of Fe-enriched aeolian material into the ocean due to the enhanced atmospheric circulation [4, 20].

The increase in the PF abundance up to maximum values, which are ~100 times higher than those during the MIS 3–LGM; the synchronous low-amplitude spike of BF abundance; and the high proportion of *G. bulloides* (up to 30%) reflect the enhanced bioproductivity at the beginning of the deglaciation, i.e. 20–19 kyr BP (Fig. 2). This event was never reported before neither in the northwestern Pacific area nor in adjacent marginal seas (Bering Sea and Sea of Okhotsk). Such a high-amplitude peak cannot be explained only by an improvement of PF preservation.

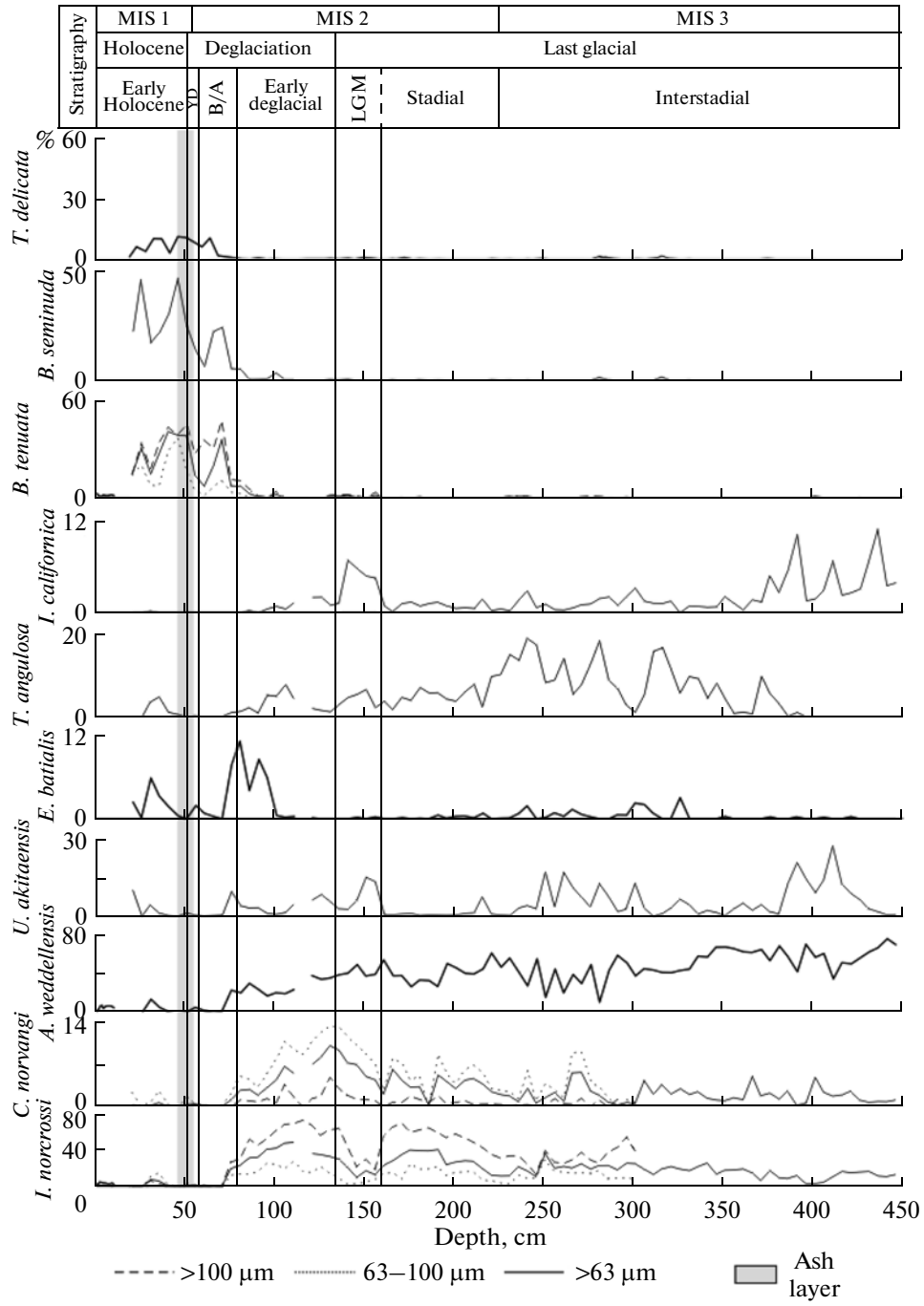


**Fig. 4.** The distribution of the most indicative benthic foraminiferal species in >100, 63–100, and >63 μm size fractions. For the legend, see Fig. 2.

According to [14, 32], the bioproductivity increased in the North Pacific later, approximately 17 kyr BP, due to the enhanced input of warm surface water of the Alaska Current and more vigorous vertical mixing, which stimulated upwelling of nutrient-rich deep water. The bioproductivity rise in the Shirshov Ridge area might be related to the longer ice-free summer seasons at the site location due to northward migration of the sea-ice margin. The documented significant increase in PF abundance likely results from the above-mentioned reorganization in the paleocirculation. If so, the latter started immediately after the LGM, i.e. considerably earlier than it is assumed in [15] for the North Pacific and in [8] for the Bering Sea.

The taxonomic composition of the BF assemblages from the sediments of the early deglaciation 20.0–14.8 kyr BP and the early Bølling/Allerød 14.8 to ~14.2 kyr BP does not differ significantly from that in the glacial

Oxygen-related benthic foraminiferal groups according to the classification by [24] and [2]. The limits of the oxygen concentrations in the bottom water for each group are given after [24]

| Oxygen-related groups | | | | |
|---|---|---|---|---|
| Oxic | Suboxic B | | Suboxic C | Dysoxic |
| 6.0–1.5 mL/L $O_2$ | 1.5–0.3 mL/L $O_2$ | | | 0.3–0.1 mL/L $O_2$ |
| Epifaunal | Infaunal | | | |
| | 0–2 cm below sea bottom | | 2–4 cm below sea bottom | >4–10 cm below sea bottom |
| *Pyrgo* spp. | *Elphidium* spp. | *Islandiella norcrossi* | *Elphidium clavatum* | *Bulimina tenuata* |
| *Lobatula lobatula* | *Uvigerina* spp. | *Islandiella californica* | *Pullenia subcarinata* | *Bolivina* spp. |
| *Miliolinella* sp. | *Takayanagia delicata* | *Alabaminella weddellensis* | *Nonionella* spp. | *Brizalina* spp. |
| *Triloculina* sp. | *Cassidulina* spp. | *Pseudoparrella takayanagii* | *Nonionellina labradorica* | *Globobulimina auriculata* |
| *Quinqueloculin*a sp. | *Cassidulinoides* sp. | *Pseudoparrella suttuensis* | *Valvulineria ochotica* | *Protoglobobulimina pupoides* |
| *Planulina ariminensis* | *Angulogerina angulosa* | *Epistominella* spp. | | *Nonionella digitata* |
| | *Melonis barleeanus* | *Cibicidoides mundulus* | | *Chilostomella fimbriata* |
| | *Stainfortia concava* | *Buccella* spp. | | *Fursenkoina* spp. |
| | *Polymorphina* spp. | *Fissurina* spp. *Ehrenbergina trigona* | | |
| | *Lagena* spp. | *Dentaina* spp. | | |
| | *Karreriella baccata voraginis* | *Oolina* spp. | | |
| | *Islandiella limbata* | *Lenticulina* sp. | | |

sediments (Fig. 4). Despite the increased surface bioproductivity at the early deglaciation, the organic matter flux to the bottom was not high enough to induce competition between glacial and postglacial BF assemblages.

The next maximum of the surface-water productivity corresponds to the middle Bølling/Allerød interstadial (~14.2 to 13.0 kyr BP). It is inferred from the increased BF and PF abundances and significant taxonomic changes in the BF assemblages, i.e. replacement of the glacial assemblage by the postglacial one with dominance of high-productivity species (Figs. 2, 4). It should be noted that the amplitude of the PF abundance spike and the content of *G. bulloides* in this interval are lower than those during the early deglaciation most likely due to the stronger dissolution (Fig. 2). The bioproductivity rise during the Bøllng/Allerød is recorded by different proxy time series from the northwestern Pacific [15], other parts of the Bering Sea [7, 8, 12, 16, 17, 18, 26] and the Sea of Okhotsk [16]. However, the causes of productivity increase are still obscure. We argue that the peaks of PF and BF abundances reflecting an increase in bioproductivity during mid-Bølling/Allerød were related to the intensified advection of nutrients by the surface currents from the gradually flooded northeastern shelf of the sea during the glacioeustatic sea level rise. Alternatively, nutrients supply to the euphotic layer could be associated with the intervals of the intense vertical mixing as it is suggested by some authors [15, 18]. The transition from the Bølling/Allerød to the Younger Dryas is marked by relatively low total PF and BF abundances (Fig. 2) probably caused by a decrease in surface-water productivity.

In the early Holocene (11.7–7.5 kyr BP), the maximum of BF abundance, prevalence of high-productivity species, a slight increase in the PF abundance, relatively poor PF preservation, and high percentages of *G. bulloides* (Fig. 2) likely reflect the maximum of primary production. This interval corresponds to the

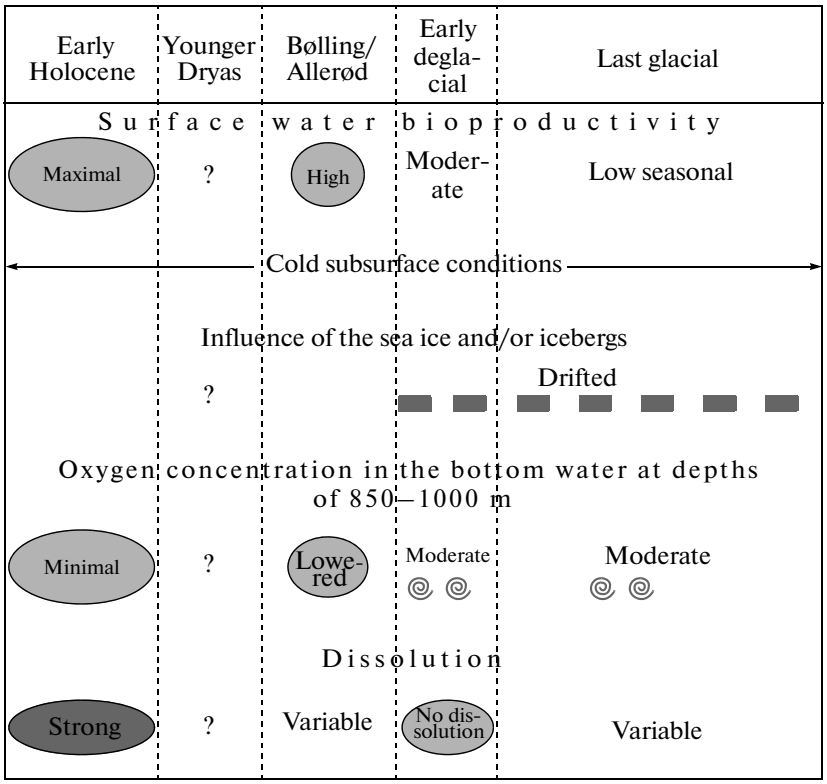


**Fig. 5.** Scheme of the paleooceanographic changes in the Shirshov Ridge area from 50 to 7.5 kyr BP.

Holocene thermal optimum that occurred in the Beringia region at 11.5–9.0 kyr BP [10]. The warm euphotic layer during summer and availability of nutrients transported to the western part of the sea from the flooded shelf provided favorable conditions for massive phytoplankton blooms. The early Holocene productivity spike is documented in the northwestern Pacific [15] and in other parts of the Bering sea [7, 8, 12, 16–18, 26] and the Sea of Okhotsk [16].

**Oxygen content in the bottom water.** Inasmuch as the oxic BF group (table) consists of species living either on the sediment surface or on the elevated substrate, we believe that their proportion may be used to reconstruct variations in the bottom-water oxygen content near the sediment–water interface. The suboxic B group of BF is represented by epifaunal and shallow infaunal species (table) and, thus, their distribution reflects changes in the oxygen concentration both at the sediment–water interface and in the pore water of upper centimeters of the sediment. In the case of low-oxygen conditions in the pore water, some species of this group might migrate towards the surface, where oxygen is available [23]. Thus, variations in the relative abundance of the suboxic B group can be also used to reconstruct the bottom water ventilation. The variability of the dysoxic group represented by the deep infaunal species reflects changes in the pore-water oxygenation. It should be kept in mind that many species of the dysoxic group respond to changes in the food flux rather than to the oxygen concentrations [23].

The insignificant content (up to 3%, Fig. 3) of the oxic BF group in the studied part of the core points to weak ventilation of the bottom water from 50 to 7.5 kyr BP. The high Fe/S values indicate that the sulfate reduction was practically absent during MIS 3–LGM; i.e., the conditions were oxidizing in the surface sediment layer. Judging by the high contents of the suboxic B group and *Angulogerina angulosa* (Figs. 3, 4), the bottom water was moderately ventilated during the MIS 3–early deglaciation and at the end of Bølling/Allerød. The relatively high oxygen content in the bottom water was likely caused by a weakening of the oxygen minimum zone due to brine rejection during the sea ice formation over the Bering Sea shelf [26] and in the Shirshov Ridge area [31]. The high content of dysoxic species (table) and the low F/S values reflecting the intensification of early diagenetic sulfate reduction in the sediments indicate oxygen-depleted conditions in the pore water during the mid-Bølling/Allerød and early Holocene. Occurrence of the suboxic B group in the Bølling/Allerød sediments implies that the oxygen content in the bottom water decreased insignificantly, if at all, and could not suppress the development of the benthic foraminiferal species of this group.

The slight decrease in proportion of the dysoxic group and synchronous increase in content of suboxic B group at Bølling/Allerød –Younger Dryas boundary

reflect the higher bottom water (at a depth of approximately 900 m) and pore water oxygenation probably due to the intensified sea ice formation on the northwestern shelf of the sea and in the Shirshov Ridge area (Fig. 3).

The negligible values of the suboxic B group during the early Holocene (Fig. 3) implies the lower oxygen content in the bottom water at that time, as compared to the Bølling/Allerød interstadial. The decreased oxygen content in the intermediate water of the western Bering Sea is explained by the ceased winter convection in this area due to the freshening of surface-water layer in response to the warming and ice melting [26, 31]. Oxygen was consumed by the oxidation of abundant organic matter on the bottom [34]. Oxygen deficiency at the intermediate water depths during the Bølling/Allerød and early Holocene is also recorded in the northeastern Bering Sea [26] and the Sea of Okhotsk [2].

**Variations in sea ice conditions** were reconstructed based on the abundance of gravel grains, proportions of terrigenous, volcanogenic, and biogenic materials in 63–100, >100, and >63 μm size fractions, and grain-size distribution (Fig. 2). The prevalence of terrigenous grains over biogenic material and the presence of gravel grains in glacial and early deglacial sediments imply development of sea ice in the Shirshov Ridge area. This is consistent with the conclusions in [25, 31]. The low concentration of gravel grains is likely explained by the scarcity of sea ice because it drifted manly within the East Kamchatka Current during spring melting, i.e., westward of the core location [9]. The occurrence of angular and subangular rock fragments, including gravel-sized grains, implies the distribution of both icebergs and sea ice in the western part of the Bering Sea during the MIS 3–early deglaciation (Fig. 5). This finding is in line with the previous conclusions that terrigenous material was transported by sea ice [16] and icebergs [9]. As shown in [9, 40], the northeastern coast of Eurasia served as a source of relatively coarse-grained terrigenous material in the North Pacific sediments.

As follows from the low content of terrigenous material and the absence of gravel, the Shirshov Ridge area was ice- and iceberg- free during the Bølling/Allerød and early Holocene.

## CONCLUSIONS

The presented reconstructions of the paleoceanographic conditions in the western Bering Sea are generally consistent with the previously obtained results from other areas of the basin [7, 8, 12, 16, 17]. The new data on the benthic foraminiferal assemblages first reveal variations in the ventilation of the bottom water in the Shirshov Ridge area at depths of 900–1000 m. The moderate oxygen content in the bottom water and the low sea surface bioproductivity are characteristic of the MIS 3–LGM. The peak in PF abundance at the onset of the deglaciation is explained by an increase in productivity and likely reflects the enhanced vertical mixing due to the early reorganization of the oceanic circulation. The PF and BF abundance peaks in the middle Bølling/Allerød interstadial and the early Holocene were caused by high productivity and sufficient food supply to the sea floor due to the high concentrations of nutrients in the mixed layer. These intervals were also characterized by an oxygen-depleted conditions in the pore and bottom water at intermediate depths. The maximum bioproductivity and minimum oxygen concentrations in the bottom water are reconstructed for the early Holocene. Coarse-grained terrigenous material was likely transported to the western part of the Bering Sea during the MIS 3–early deglaciation by both icebergs and drifted sea ice.

## ACKNOWLEDGMENTS

We thank I.O. Murdmaa, M.P. Chekhovskaya, Kh.M. Saidova, N.V. Bubenshchikova, T.A. Khusid, and I.N. Sukhanova for discussions and recommendations, and E. Kandiano for the help with application of factor analysis. This work was conducted in the framework of the Russian–German KALMAR Project and supported by the OSL-10-14, OSL-11-11, and OSL-12-15 projects of the Otto Schmidt Laboratory of Polar and Marine Research; the Program of Basic Research (no. 21, "Basic Problems of Oceanography: Physics, Geology, Biology, Ecology") of the Presidium of the Russian Academy of Sciences, and the Russian Foundation for Basic Research (projects 12-05-00617_a and 12-05-31118 mol_a).

## REFERENCES

1. V. S. Arsen'ev, *Currents and Water Masses of the Bering Sea* (Nauka, Moscow, 1967) [in Russian].
2. N. V. Bubenshchikova, D. Nürnberg, S. A. Gorbarenko, and L. Lembke-Jene, "Variations of the Oxygen Minimum Zone of the Okhotsk Sea during the Last 50 ka as Indicated by Benthic Foraminiferal and Biogeochemical Data," Oceanology **50** (1), 93–106 (2010).
3. I. I. Burmistrova, M. P. Chekhovskaya, and N. V. Belyaeva, "Benthic Foraminifers in Eastern Slope of the Bering Seas," Oceanology **44** (5), 734–742 (2004).
4. S. A. Gorbarenko and E. L. Gol'dberg, "Assessment of Variations of Primary Production in the Sea of Okhotsk, Bering Sea, and Northwestern Pacific over the Last Glaciation Maximum and Holocene," Dokl. Earth Sci. **405A** (9), 1380–1383 (2005).
5. A. P. Lisitsyn, *Current Sedimentation Processes in the Bering Sea* (Nauka, Moscow, 1966) [in Russian].
6. Kh. M. Saidova, *Ecology of Foraminifers and Paleogeography of the Far East Seas of USSR and Northwestern Pacific* (Akad. Nauk SSSR, Moscow, 1961) [in Russian].

7. T. A. Khusid, I. A. Basov, S. A. Gorbarenko, and M. P. Chekhovskaya, "Benthic Foraminifers in Upper Quaternary Sediments of the Southern Bering Sea: Distribution and Paleoceanographic Interpretations," Stratigr. Geol. Correl. **14** (5), 538–548 (2006).
8. M. P. Chekhovskaya, I. A. Basov, A. G. Matul, T. A. Khusid, and S. A. Gorbarenko, "Planktonic Foraminifers in the Southern Bering Sea: Changes in Composition and Productivity during the Late Pleistocene – Holocene," Stratigr. Geol. Correl. **16** (3), 328–342 (2008).
9. G. R. Bigg, C. D. Clark, and A. L. C. Hughes, "A Last Glacial Ice Sheet on the Pacific Russian Coast and Catastrophic Change Arising from Coupled Ice-Volcanic Interaction," Earth Planet. Sci. Lett. **265**, 559–570 (2008).
10. B. E. Caissie, J. Brigham-Grette, K. T. Lawrence, et al., "Last Glacial Maximum to Holocene Sea Surface Conditions at Umnak Plateau, Bering Sea, as Inferred from Diatom, Alkenone, and Stable Isotope Records," Paleoceanography **25**, PA1206 (2010). doi 10.1029/2008PA001671.
11. R. Chen, Y. Meng, R. Wang, D. Hua, and J. Xu, "Oceanographic Records of Microorganisms in the Surface Sediments from the Bering and Chukchi Seas," Asian J. Water, Environ. Pollut. **2** (1), 19–26 (2005).
12. M. S. Cook, L. D. Keigwin, and C. A. Sancetta, "The Deglacial History of Surface and Intermediate Water of the Bering Sea," Deep-Sea Res., Part II **52**, 2163–2173 (2005).
13. K. F. Darling and C. M. Wade, "The Genetic Diversity of Planktic Foraminifera and the Global Distribution of Ribosomal RNA Genotypes," Marine Micropaleontology **67**, 216–238 (2008).
14. *SO201-KALMAR Leg 2 Cruise Report No. 35,* Ed. by W.-C. Dullo, B. Baranov, and C. van den Bogaard (IFM-GEOMAR, Germany, 2009).
15. H. Gebhardt, M. Sarnthein, P. M. Grootes, et al., "Paleonutrient and Productivity Records from the Subarctic North Pacific for Pleistocene Glacial Terminations I to V," Paleoceanography **23**, PA4212 (2008). doi 10.1029/2007PA001513.
16. S. A. Gorbarenko, "Stable Isotope and Lithological Evidence of Late-Glacial and Holocene Oceanography of the Northwestern Pacific and Its Marginal Seas," Quaternary Res. **46**, 230–250 (1996).
17. S. A. Gorbarenko, I. A. Basov, M. P. Chekhovskaya, et al., "Orbital and Millennium Scale Environmental Changes in the Southern Bering Sea during the Last Glacial-Holocene: Geochemical and Paleontological Evidence," Deep-Sea Res., Part II **52**, 2174–2185 (2005).
18. S. A. Gorbarenko, P. Wang, R. Wang, and X. Cheng, "Orbital and Suborbital Environmental Changes in the Southern Bering Sea during the Last 50 kyr," Palaeogeogr., Palaeoclimatol., Palaeoecol. **286**, 97–106 (2010).
19. M. Hald, C. Andersson, H. Ebbesen, et al., "Variations in Temperature and Extent of Atlantic Water in the Northern North Atlantic during the Holocene," Quat. Sci. Rev. **26**, 3423–3440 (2007).
20. J. C. Herguera, T. Herbert, M. Kashgarian, and C. Charles, "Intermediate and Deep Water Mass Distribution in the Pacific during the Last Glacial Maximum Inferred from Oxygen and Carbon Stable Isotopes," Quat. Sci. Rev. **29**, 1228–1245 (2010).
21. J. Imbrie and N. G. Kipp, "A New Micropaleontological Method for Quantitative Paleoclimatology: Application for a Late Pleistocene Caribbean Core," in *The Late Cenozoic Glacial Ages*, Ed. by K. Turikian (Yale Univ. Press, New Haven, 1971), pp. 71–181.
22. S. L. Jaccard, G. H. Haug, D. M. Sigman, et al., "Glacial/Interglacial Changes in Subarctic North Pacific Stratification," Science **308**, 1003–1006 (2005).
23. F. J. Jorissen, C. Fontanier, and E. Thomas, "Paleoceanographical Proxies Based on Deep-Sea Benthic Foraminiferal Assemblage Characteristics," in *Proxies in Late Cenozoic Paleoceanography, Part 2: Biological Tracers and Biomarkers*, Ed. by C. Hillaire-Marcel and A. de Vernal (Elsevier, Amsterdam, 2007), pp. 263 – 325.
24. K. Kaiho, "Benthic Foraminiferal Dissolved-Oxygen Index and Dissolved-Oxygen Levels in the Modern Ocean," Geology **22**, 719–722 (1994).
25. K. Katsuki and K. Takahashi, "Diatoms as Paleoenvironmental Proxies for Seasonal Productivity, Sea-Ice and Surface Circulation in the Bering Sea during the Late Quaternary," Deep-Sea Res., Part II **52**, 2110–2130 (2005).
26. S. Kim, B. K. Khim, M. Uchida, et al., "Millennial-Scale Paleoceanographic Events and Implication for the Intermediate-Water Ventilation in the Northern Slope Area of the Bering Sea during the Last 71 Kyrs," Global and Planetary Change **79**, 89–98 (2011).
27. K. Kohfeld and Z. Chase, "Controls on Deglacial Changes in Biogenic Fluxes in the North Pacific Ocean," Quat. Sci. Rev. **30**, 3350–3363 (2011).
28. K. E. Kohfeld and R. G. Fairbanks, "*Neogloboquadrina pachyderma* (Sinistral Coiling) as Paleoceanographic Tracers in Polar Oceans: Evidence from Northeast Water Polynya Plankton Tows, Sediment Traps, and Surface Sediments," Paleoceanography **11** (6), 679–699 (1996).
29. S. A. Korsun and M. Hald, "Modern Benthic Foraminifera off Novaya Zemlya Tidewater Glaciers, Russian Arctic," Arct. Alp. Res. **30** (1), 61–77 (1998).
30. V. Luchin, V. Menovshchikov, and V. E. Lavrentiev, "Thermohaline Structure and Water Masses in the Bering Sea," in *Dynamics of the Bering Sea*, Ed. by T. R. Loughlin and K. Ohtani (Univ. of Alaska Sea Grant, Fairbanks, 1999), pp. 61–91.
31. L. Max, J.-R. Riethdorf, R. Tiedemann, et al., "Sea Surface Temperature Variability and Sea-Ice Extend in the Subarctic Northwest Pacific during the Past 15 000 Years," Paleoceanography **27**, PA3213 (2012). doi 10.1029/2012PA002292.
32. Y. Okazaki, A. Timmermann, L. Menviel, et al., "Deepwater Formation in the North Pacific during the Last Glacial Termination," Science **329**, 200–204 (2010).
33. J. D. Ortiz, A. C. Mix, and R. W. Collier, "Environmental Control of Living Symbiotic and Asymbiotic

Foraminifera of the California Current," Paleoceanography **10** (6), 987–1009 (1995).

34. J.-R. Riethdorf, L. Max, D. Nürnberg, and R. Tiedemann, "Late Pleistocene to Holocene Changes in Sea Surface Temperature, Marine Productivity and Terrigenous Fluxes in the Western Bering Sea," in *Abstracts of the KALMAR Workshop* (Trier, Germany, 2011), pp. 105–107.
35. G. I. Roden, "Flow and Water Property Structures between the Bering Sea and Fiji in the Summer of 1993," J. Geophys. Res. **105** (C12), 28595–28612 (2000).
36. B. K. Sen Gupta and M. L. Machain-Castillo, "Benthic Foraminifera in Oxygen-Poor Habitats," Marine Micropaleontology **20**, 83–201 (1993).
37. A. M. Springer, C. P. McRoy, and M. V. Flint, "The Bering Sea Green Belt: Shelf-Edge Processes and Ecosystem Production," Fisheries Oceanography **5** (3/4), 205–223 (1996).
38. P. J. Stabeno, J. D. Schumacher, and K. Ohtani, "The Physical Oceanography of the Bering Sea," in *Dynamics of the Bering Sea*, Ed. by T. R. Loughlin and K. Ohtani, (Univ. of Alaska Sea Grant, Fairbanks, 1999), pp. 1–21.
39. R. Stein, *Arctic Ocean Sediments: Processes, Proxies, and Paleoenvironment* (Elsevier, Amsterdam, 2008).
40. K. E. K. John, St. and L. A. Krissek, "Regional Patterns of Pleistocene Ice-Rafted Debris Flux in the North Pacific," Paleoceanography **14**, 653–662 (1999).
41. E. Thomas, E. Booth, M. Maslin, and N. J. Shackleton, "Northeastern Atlantic Benthic Foraminifers during the Last 45 000 Years: Changes in Productivity Seen from the Bottom Up," Paleoceanography **10**, 545–562 (1995).
42. J. Zhang, R. Woodgate, and R. Moritz, "Sea Ice Response to Atmospheric and Oceanic Forcing in the Bering Sea," J. Phys. Oceanogr., No. 40, 1729–1747 (2010).